Quantum Electronics **42** (7) 567–574 (2012)

LASERS

PACS numbers: 42.65.Yj; 42.55.Rz; 42.65.Re; 42.60.By
DOI: 10.1070/QE2012v042n07ABEH014689

High-energy Nd:YAG-amplification system for OPCPA pumping*

J. Adamonis, R. Antipenkov, J. Kolenda, A. Michailovas, A.P. Piskarskas, A. Varanavičius

Abstract. **We present a high-energy picosecond Nd:YAG-amplification system seeded with pulses of a femtosecond Yb:KGW oscillator. The Nd:YAG amplifier is intended to pump an optical parametric chirped-pulse amplification (OPCPA) system. Generation of high contrast pulses with energy of 600 mJ and pulse duration of 100 ps is demonstrated.**

Keywords: *optical parametric chirped pulse amplification system, intracavity etalon, improved contrast.*

1. Introduction

There is a growing interest in the development of optical parametric chirped pulse amplification (OPCPA) systems for a range of applications requiring ultrahigh-power few cycle optical pulses [1]. A high-energy picosecond-pulse amplifier system usually consisting of regenerative and linear amplifiers, providing high quality pulses for pumping parametric amplifiers is one of the key components of such systems [2, 3]. It is shown [4] that for a few-cycle OPCPA, picosecond pump pulses are superior to nanosecond pump pulses due to larger parametric amplification bandwidth, higher damage threshold of nonlinear crystals, and better amplified chirped pulse recompression. On the other hand, shorter picosecond pulse durations toughen requirements to the accuracy of pump pulse synchronisation.

Because in a chirped pulse different spectral components are distributed on the pulse envelope, OPCPA requires accurate synchronisation of the pump and signal pulses to ensure their temporal overlapping during parametric amplification [5]. Thus, to realise all-optical signal–pump synchronisation, the seed for the pump laser should be derived from a femtosecond master oscillator [6]. Ti:sapphire femtosecond oscillators widely used in OPCPA systems operate outside the gain region of picosecond (Nd:YAG, Nd:YLF, Nd:YVO) pump amplifiers. For this reason, successful seeding of Nd^{3+}-doped regenerative amplifiers (RAs) requires octave-spanning chirped-mirror Ti:sapphire oscillators [4], or an additional external nonlinear photonic crystal fibre which frequency shifts Ti:sapphire oscillator spectrum to Nd^{3+} fluorescence line [7].

Nevertheless, by using both seeding techniques, the maximum delivered seed energy at 1064 nm was less than 2 pJ. It is widely known, that insufficient seed energy results in a low amplified pulse contrast level, defined as the ratio of the pulse peak intensity to the intensity of amplified spontaneous emission (ASE). Deteriorated contrast at the output of amplifiers may severely reduce usable energy in the amplified picosecond pulse [4] and lead to the appearance of a pedestal of compressed pulses at the output of the OPCPA system [8]. Another promising OPCPA pump amplifier seeding method is seeding with a femtosecond Yb:KGW oscillator, delivering significant part of 1064 nm radiation for Nd^{3+} amplifiers. Seeding of Nd:YAG amplifiers with Yb:KGW pulses was demonstrated for the first time in [9], but the amplified pulse contrast with respect to ASE was not investigated.

In this paper we report for the first time contrast measurements for Yb:KGW pulses amplified in a picosecond Nd:YAG amplifier system. Furthermore, we concentrated on picosecond pulse temporal profile formation by using multiple intracavity etalons. For output pulse contrast enhancement we applied pulse cleaning technique based on intensity dependent fundamental pulse polarisation rotation in a phase-matching type-II second harmonic generator operating under conditions of unbalanced intensities of input polarisation components. The use of this effect for fabricating a device exhibiting intensity dependent transmission was demonstrated for the first time by Leford and Barthelemy [10] and was employed in a setup of an all-optical transistor [11] and various mode-locking schemes [12–14]. To our knowledge it is the first time when such a technique has been implemented for picosecond pulse contrast enhancement.

2. Seeding of Nd:YAG amplifiers with pulses of a femtosecond Yb:KGW oscillator

The key feature of our system is the direct seeding of Nd:YAG amplifiers with femtosecond pulses of a Yb:KGW oscillator which is simultaneously used to pump and seed an optical parametric amplifier (OPA). Such an approach ensures reliable all-optical pump–signal synchronisation in OPCPA system stages. In our setup (see Fig. 1), the femtosecond Yb:KGW oscillator (Light conversion Ltd., Lithuania) which generates 60-fs, 9-nJ pulses at a 78-MHz repetition rate

* Reported at the conference 'Laser Optics 2010', St. Petersburg, Russia.

J.Adamonis. Vilnius University, Faculty of Physics, Department of Quantum Electronics, Saulėtekio al. 9, LT-10222 Vilnius, Lithuania; UAB 'Ekspla', Savanorių 231, LT-02300 Vilnius, Lithuania; e-mail: j.adamonis@ekspla.com
R.Antipenkov, A.P.Piskarskas, V.Varanavičius. Vilnius University, Faculty of Physics, Department of Quantum Electronics, Saulėtekio al. 9, LT-10222 Vilnius, Lithuania;
J.Kolenda, A.Michailovas. UAB 'Ekspla', Savanorių 231, LT-02300 Vilnius, Lithuania; Center for Physical Sciense and Technology, Savanorių 231, LT-02300 Vilnius, Lithuania

Received 18 October 2011; revision received 15 May 2012
Kvantovaya Elektronika **42** (7) 567–574 (2012)
Translated by A. Michailovas

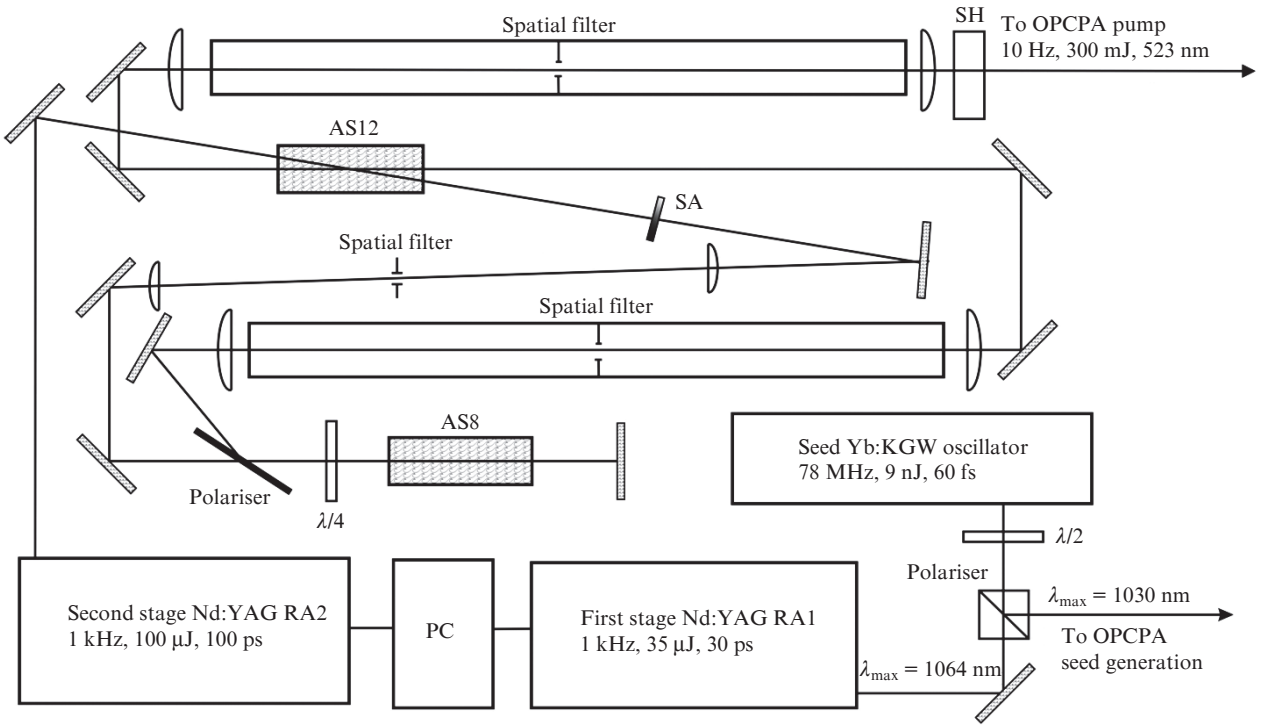

Figure 1. Schematic of the Nd:YAG amplification system: (SA) serrated aperture; (SH) second harmonic crystal; (PC) pulse cleaner; [AS12 (8)] Nd:YAG amplification stage with an AE diameter of 12 mm (8 mm).

was used as a seed source. A part of the oscillator output was coupled into the Nd:YAG amplification system, remainder of the pulse was used as a seed for the femtosecond Yb:KGW amplifier. High-order half-wave plate and polarisation cube were used as a spectrally selective beam splitter. The Yb:KGW and Nd:YAG amplifiers operated at different wavelengths, namely 1030 nm and 1064 nm. To realise a spectrally selective polarisation beam splitter, the phase retardation quartz plate of special design was fabricated inducing a phase shift of 2π at 1064 nm and of π at 1030 nm. As a result, the spectral component at 1030 nm changed the polarisation state into orthogonal due to the polarisation cube and was coupled into the Yb:KGW RA (Fig. 2). The spectral component, which preserved its polarisation state at 1064 nm, was coupled into the Nd:YAG RA.

The estimated seed energy within the fluorescence bandwidth of the Nd:YAG centred at 1064 nm was 12 pJ. The 1-kHz repetition rate RA1 (UAB 'EKSPLA' Ltd, Lithuania) was based on the Nd:YAG rod ($\varnothing 6 \times 10$ mm) pumped by a 3-W cw laser diode. The maximum amplified pulse energy of 35 μJ was limited by the Kerr effect and resistance to radiation damage of the Nd:YAG rod coating. In order to examine the amplified picosecond pulse contrast (the ratio of the nanosecond ASE background and main pulse intensities), we performed a series of high dynamic range third-order correlation measurements using 3ω THC Sequoia autocorrelator (Amplitude Technologies, France) (Fig. 3a). During these measurements we varied the seed energy and correspondingly adjusted the cavity dumping time, thereby maintaining approximately the same amplified pulse energy.

We consider that a nanosecond Q-switched pulse is background. Assuming that the ASE intensity is flat in time with duration equal to the RA cavity round trip time (~12 ns), the background pulse contained about 0.015 % of the total amplifier RA1 output energy, when the pulse intensity contrast was 4×10^{-7}. For further pulse amplification up to 100 μJ and pulse temporal intensity profile formation (see Section 4) we used the second stage regenerative amplifier (RA2), similar to RA1. One can see from Fig. 3b that the pulse contrast at the RA2 output was at level of $\sim 3 \times 10^{-6}$. Taking into account the fact that at the RA2 output the pulse duration was about 100 ps and ASE pedestal duration was 12 ns, the calculated ASE background energy contains approximately 0.036% of the total output energy. This energy contrast value is about 2.4 times worse than in RA1. We suppose that drop of the contrast is caused by additional quantum noises and gain saturation in the RA2 laser rod. Nevertheless, the measured intensity contrast value (3×10^{-6}) is about 10^2 times better

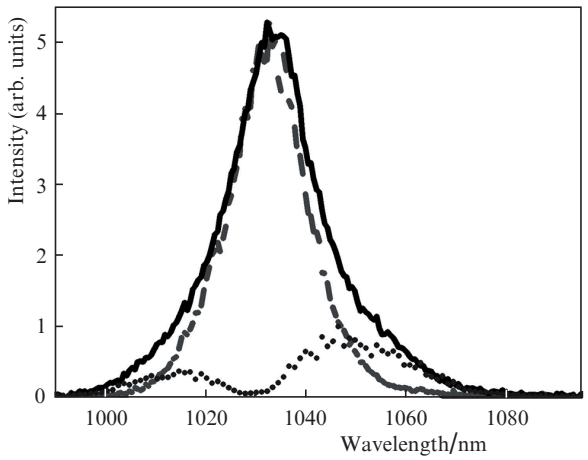

Figure 2. Emission spectrum of the Yb:KGW oscillator (solid line), seed pulses coupled into Nd:YAG RA (dotted line) and seed pulses coupled into Yb:YAG RA (dashed line).

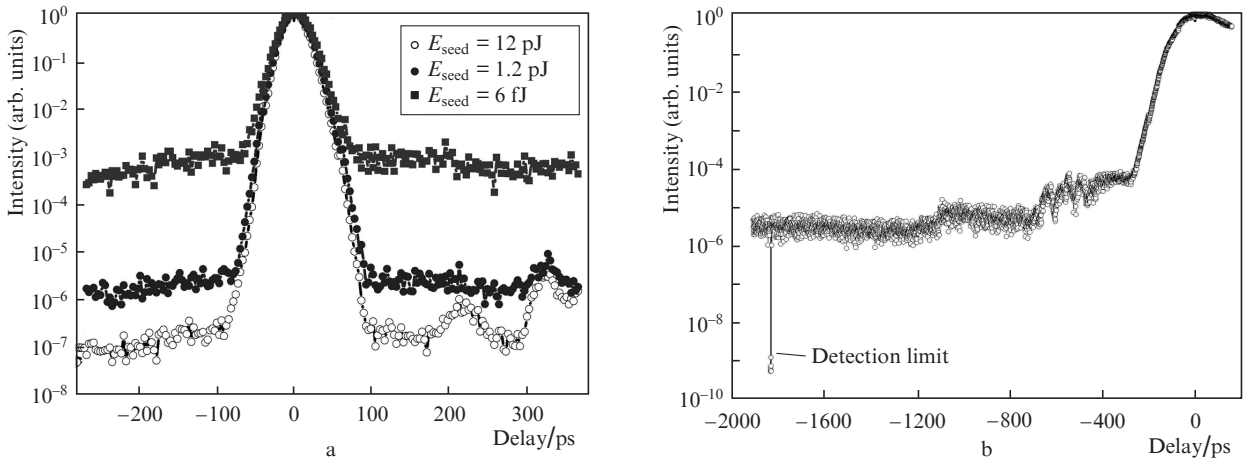

Figure 3. Third-order correlation traces of pulses amplified in RA1 (a) and RA2 (b).

than the results published on the contrast ratio in the Nd^{3+} RA seeded with soliton-shifted pulses from a femtosecond Ti:sapphire oscillator [4].

3. Shaping of a spatial beam profile

The pump beam profile is one of the critical issues in high energy OPCPA system development. First of all, the spatial beam profile should be uniform to ensure uniform intensity distribution of the amplified signal beam profile. Furthermore, the beam profile must provide maximal extraction of the energy stored in active elements (AEs) at a safe level of the output peak intensity. On the other hand, when the beam cross section significantly exceeds the AE cross section, diffraction from the AE edges can initiate small-scale self-focusing and lead to AE damage. It is shown [15] that the top-hat beam profile (super-Gaussian beam distribution) is the best solution to the above requirements. We have designed a beam shaping system using a serrated pattern aperture followed by an imaging spatial filter. The plane of the aperture was relay imaged to the entrance plane of the rod AE of the amplification stage (∅8 mm). The diameter d_{ap} of the spatial filter aperture was chosen following criteria $d_{ap} < d$, where $\frac{1}{2}f\lambda/L$ [16] (f is the focal length of the first lens of the filter, L is the serration period in the aperture). The chosen aperture diameter of 0.6 mm was about five times smaller than d. Beam profiles after the aperture and in the relay imaged plane are given in Fig.4.

Before forming the spatial profile, a 100-ps pulse beam from the RA2 output passed through the 12-mm amplifier rod at a small angle to the rod axis for 10-fold pre-amplification. The Gaussian output of RA2 using the beam shaping system was transformed to an approximately second-order super-Gaussian beam (Fig. 4b). During amplification, the beam profile due to gain saturation and nonuniform amplification in the AE becomes more flattened. The final spatial beam profile after 8-mm and 12-mm amplification stages can be approximated by the third-order super-Gaussian distribution (Fig. 4c).

The amplified 600-mJ pulse was frequency doubled in a second harmonic DKDP crystal with 60% efficiency. The second harmonic crystal was placed in the relay image plane of the output of the 12-mm amplifier stage. The second harmonic beam profile at a distance of 1.5 m from the nonlinear crystal still shows no diffraction rings (Fig. 5), but exhibits some asymmetry (ellipticity factor ~0.7).

4. Formation of a temporal profile of the pulse

In order to reach maximum pump-to-signal conversion efficiency in the OPCPA system, the pump pulse duration should be matched to the chirped signal pulse duration. On the other hand, at a higher pump fluence in the parametric amplification process, a longer pulse duration is required to avoid the damage of optical elements (damage threshold is ~20 GW cm^{-2} for AR coatings). In our system femtosecond seed pulses from Yb:KGW have been temporally stretched due to gain narrowing in the RA and use of Fabry–Perot intracavity etalons (IEs) [17, 18]. It is worth mentioning that if IE double pass transit time is on the order of the input pulse duration, the RA output pulse could be temporally modulated [17]. In order to avoid this modulation multiple IEs with different thicknesses are usually used.

In order to examine the impact of single or double IE systems on the amplified pulse envelope, we performed computer modelling using the algorithm presented in [17]. The pulses in simulations were described as Gaussian ones, their phase modulation was accounted for by a linear chirp factor γ which enters the uncertainty relation for a transform-limited pulse:

$$K = \Delta\nu + \Delta\tau = 0.44\sqrt{1+\gamma^2}\,.$$

In a real picosecond RA $\gamma \neq 0$ due to nonlinear interaction of a picosecond pulse with RA cavity components. Several pulse duration formation setups were tested experimentally and theoretically. The measurements were performed with the help of a THC Sequoia system using as frequency doubled probe pulses from the Yb:KGW RA (pulse duration ~300 fs). At first stage of the experiment we inserted a 2-mm-thick single IE made of SF-6 glass with 20% reflection coatings on both surfaces. 25-ps (FWHM) output pulses from RA1 were injected to the RA2 cavity and after 9 round trips were amplified up to 100 μJ. For this particular case the input pulse duration was close to the IE double transit time (24 ps). As a consequence, the RA2 output pulse exhibits severe temporal envelope modulation (up to 0.12) which is in a good agreement with simulation results (Fig. 6).

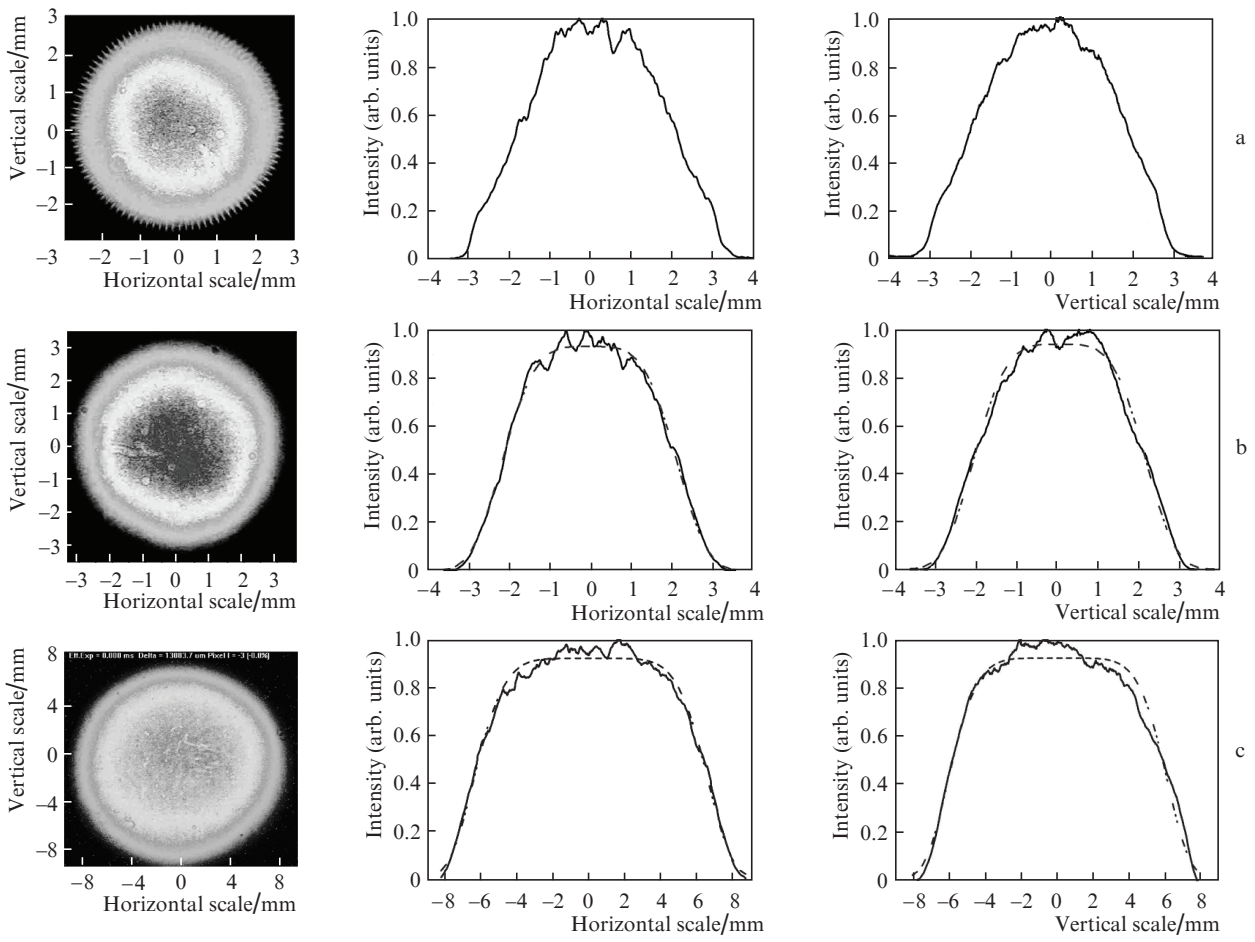

Figure 4. Spatial beam intensity distributions at a distance of 10 cm behind the serrated aperture (a), at the input of the Nd : YAG AE of the AS8 (b) and at the output of the amplification stages AS8 and AS12 (c). The pulse energy is 600 mJ. Solid lines show the spatial profile, dashed curves is the approximation by the second-order (b) and third-order (c) super-Gaussian function.

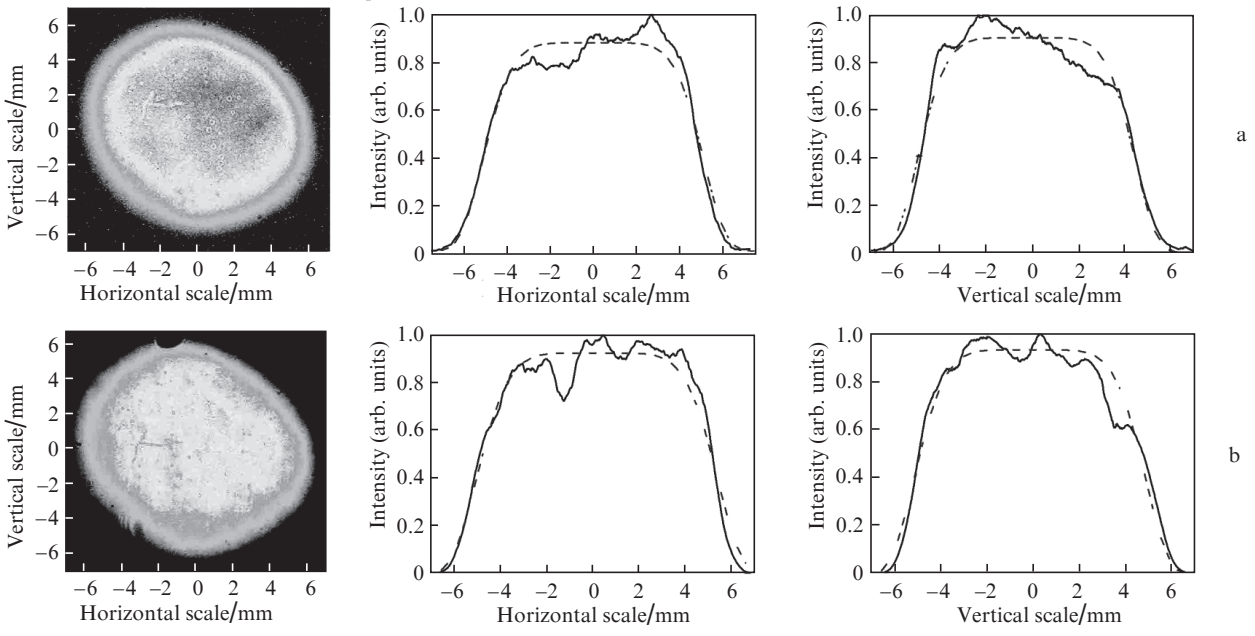

Figure 5. Spatial beam intensity distributions at a distance of 150 cm from the SH crystal for the fundamental beam profile (a) and SH beam profile (b). Solid lines show the spatial profile, dashed curves is the approximation by the third-order super-Gaussian function.

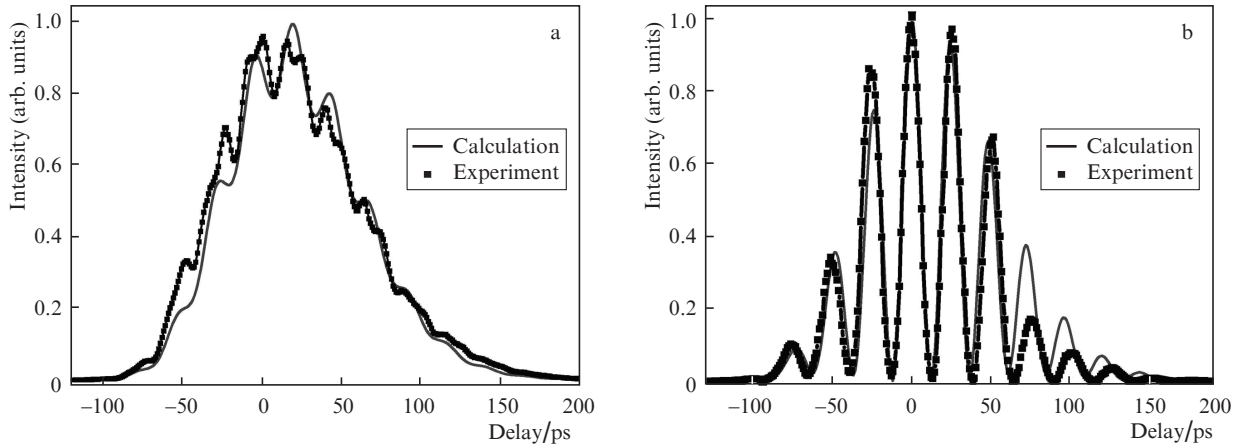

Figure 6. Pulse temporal profile at the output of RA2 with a single 2-mm-thick SF-6 glass intracavity etalon ($R_1 = 0.2$) when the etalon is tilted to resonant (a) and antiresonant position (b). In calculations the linear chirp factor $\gamma = 1$ is used, the number of round trips in the RA is 9.

Computer modelling revealed that temporal envelope modulation strongly depends on the seed pulse duration $\Delta\tau$ (Fig. 7). Virtually varying the input pulse length $\Delta\tau$ from 20 ps to 32 ps envelope modulation was reduced from 4×10^{-2} to 6×10^{-5} at $\gamma = 0$. On the other hand, the calculation shows that the magnitude of envelope modulation is strongly affected by the input seed pulse chirp γ. When $\gamma = 1.1$ and $\Delta\tau = 32$ ps, the modulation depth is 0.5×10^{-2}. This value is three orders of magnitude worse than $\gamma = 0$. The employment of the second IE in the RA cavity made it possible to reduce undesired pulse modulation (Fig. 7b). According to calculations, insertion of an additional 1-mm-thick uncoated IE (SF-6) could result in the pulse envelope modulation reduction from 0.5×10^{-2} to 7×10^{-4}. The calculated dependence of the pulse envelope modulation depth on the second IE thickness and reflectivity R_2 is presented in Fig. 8.

As seen from Fig. 8a, the optimum thickness of the second IE should be equal to half the length (1 mm in our case) of the first etalon. Another important IE parameter which impacts the modulation depth is IE surface reflectivity R_2. The increase in R_2 results in significant reduction of the modulation depth (Fig. 8b). It should be noted that introducing the second IE also affects the output pulse duration. However, the impact of the second IE on the pulse lengthening is quite weak compared with the contribution of the first IE. For instance, with changing 1-mm-thick IE reflectivity of from 0.04 to 0.3 the output pulse width increased from 95 ps to 115 ps (without accounting for gain narrowing).

On the basis of simulation results we inserted into the RA2 cavity two SF-6 etalons: the first one was 2-mm thick with 0.2 reflectivity and the second one was 1-mm thick with 0.3 reflectivity. By using this double IE system, the RA1 output pulse was stretched in time up to 100 ps without noticeable pulse modulation (see Fig. 9). According to computer simulation, the modulation depth value should not exceed 5.5×10^{-6}. Unfortunately, in the experiment the noise of THC photomultiplier did not allowed us to reach the required accuracy.

To enhance the amplified pulse contrast in respect to the ASE level, we have employed a pulse cleaner (PC) based on unbalanced second harmonic generation (SHG) [10]. Schematic of the setup is presented in Fig. 10. Linearly polarised pump radiation is directed to the type-II SHG crystal that is cut and oriented for phase-matched frequency doubling. The conversion efficiency to second harmonic and polarisation state of pump radiation at the output of the crys-

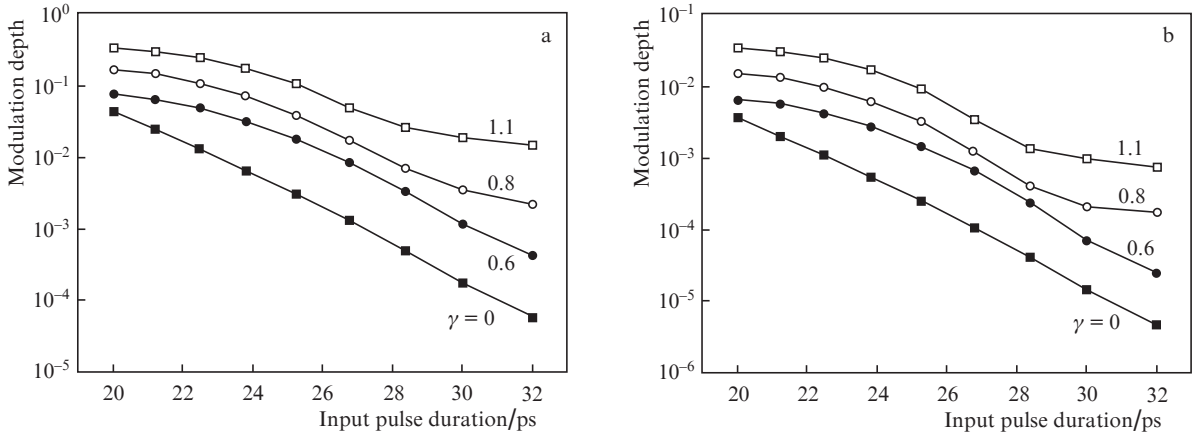

Figure 7. Calculated pulse intensity envelope modulation depth versus input pulse duration and linear chirp parameter γ for a single 2-mm-thick SF-6 glass etalon ($R_1 = 0.2$) (a) and an additional second 1-mm-thick SF-6 etalon ($R_2 = 0.07$) (b). The number of round trips in the RA is 9.

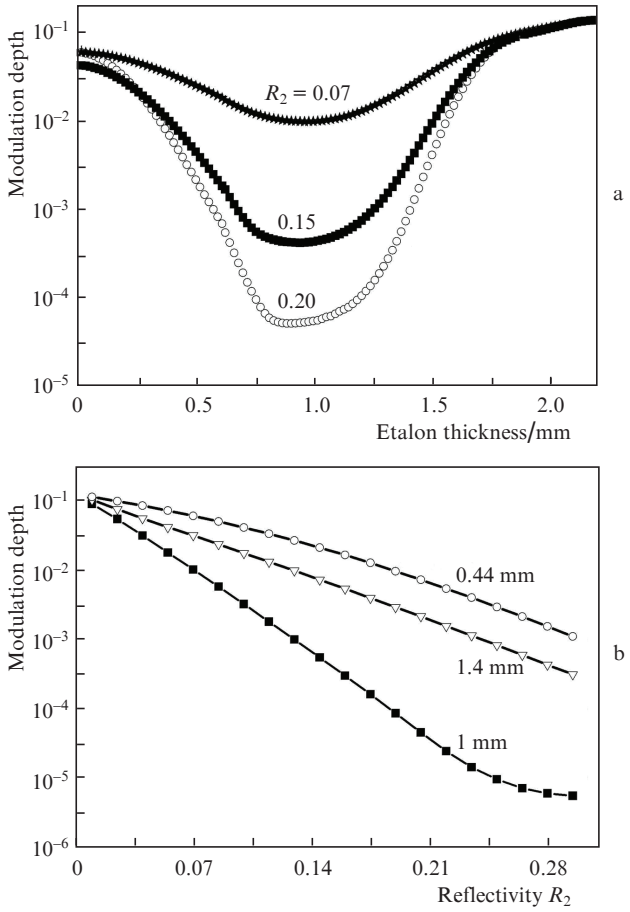

Figure 8. Calculated pulse envelope modulation depth versus the second intracavity etalon thickness (a) and surface reflectivity R_2 (b). The input pulse duration is 25 ps, the chirp parameter is $\gamma = 1.1$, the number of round trips is $n = 9$, the first intracavity SF-6 etalon thickness is 2 mm, the reflectivity is $R_1 = 0.2$.

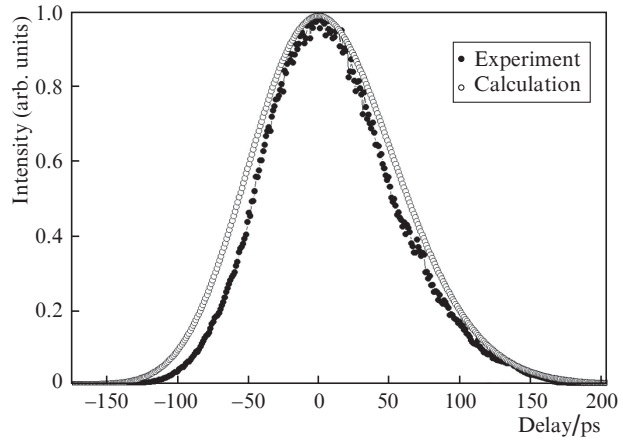

Figure 9. Temporal pulse profile at the output of RA2 with a double intracavity etalon system. In calculation the chirp factor $\gamma = 1.1$ is used.

tal depends both on the pump intensity and angle β between the pump polarisation plane and directions of the axis of the refractive index of the extraordinary (or ordinary) waves. When this angle is $\beta = 45°$, the magnitude of pump field components $\boldsymbol{E}_{in}$ of o- and e-polarisations in the crystal are equal: $\boldsymbol{E}_o = \boldsymbol{E}_e$. During the SHG these components are depleted by

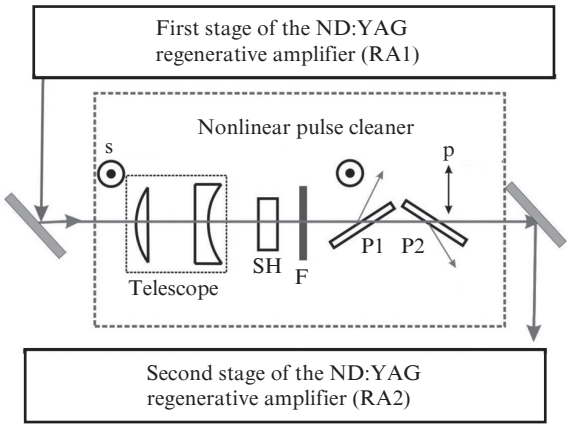

Figure 10. Schematic of the pulse cleaner setup: (P1, P2) thin film polarisers; (SH) KTP crystal for second harmonic generation; (F) SH cut off filter.

same ratio and consequently there are no changes in the state of fundamental radiation polarisation.

Situation is different when the angle β between one of the crystal indicatrix axis and polarisation direction of the fundamental field $\boldsymbol{E}_{in}$ differs from 45°: the magnitude of the pump o- and e-components $\boldsymbol{E}_o$ and $\boldsymbol{E}_e$ are unequal (Fig. 11a). Generation of the second harmonic diminishes both components $\boldsymbol{E}_o$ and $\boldsymbol{E}_e$ by the same amount. The resultant pump polarisation remains linear but experiences rotation of its plane. For a certain SHG crystal length one of these components ($\boldsymbol{E}_o$ in our case) could be completely depleted (Fig 11b) and the polarisation plane at the crystal output is rotated by angle β. For longer nonlinear interaction lengths, the frequency conversion process turns to difference frequency generation between the generated SH and the remaining fundamental component $\boldsymbol{E}_e$. The fundamental field with the plane of polarisation parallel to the 'o' axis is regenerated, but the phase of the created field is now shifted by π with respect to the initial field. At proper conditions of nonlinear interaction the magnitude of the polarisation components $\boldsymbol{E}_o$ and $\boldsymbol{E}_e$ of the pump can be fully restored (Fig 11c). In this case, the plane of radiation polarisation at the nonlinear crystal output experiences maximal rotation by the angle 2β. With a polariser installed after the SHG crystal such a setup exhibits intensity dependent transmission and could serve for enhancement of the contrast between the main pulse, possible satellites and ASE background.

In our experiment the incident beam diameter was reduced and collimated by a telescope; therefore, the beam diameter in the 3-mm-thick KTP crystal was set to ~500 μm ($1/e^2$) resulting in a maximum peak intensity of 0.88 GW cm^{-2} . The polarisation of fundamental radiation after the SHG crystal was analysed by pair of thin film polarisers while the SH was cut off by a colour glass filter. The optimum PC operation regime was set by maximising the filter transmission for picosecond pulses from RA1. The maximum PC transmission of 24% was reached at $\alpha_{in} = 15°$, where α_{in} is the angle between the pump polarisation plane and bisector of the angle between the indicatrix axes of the nonlinear crystal (dashed lines in Fig 11). At low radiation intensities the cleaner transmission was on order of 2×10^{-3}. Using simplified consideration (depicted in Fig 11) in our case for $\alpha_{in} = 15°$ the maximum polarisation rotation can reach $2\beta = 60°$ and the maximum intensity transmission of 75% can be expected. In a more

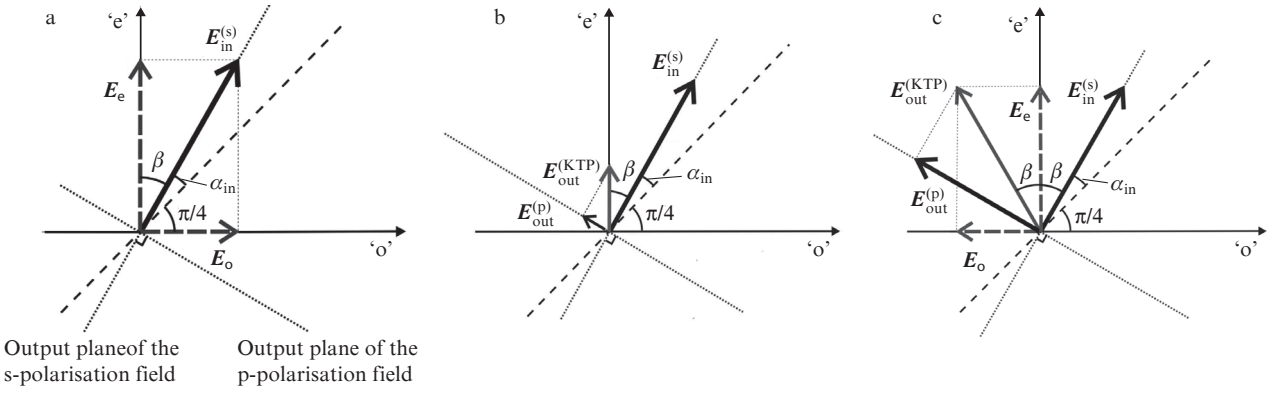

Figure 11. Vector diagram for fundamental field polarisation components in case of unbalanced SHG in the type-II phase-matching crystal: at input of the crystal (a), at full depletion of the E_o component (b), at complete regeneration of fundamental field components (c).

detailed investigation and numerical simulation of three-wave interaction according to the model presented in [10], the maximum induced transparency reached 0.65 for $\beta = 31°$, i.e., for $\alpha_{in} = 14°$. In our experimental conditions these values (and full SH reconversion) are hardly achievable due to the limited pulse energy from RA1. The use of longer crystals or more tight focusing lowers the value of pulse cleaner extinction at low radiation intensities due to higher device sensitivity to radiation divergence, intrinsic depolarisation due to crystal inhomogeneity, spatial walk-off effect. Another important aspect is that the SHG crystal in the experimental setup of pulse cleaner acts as a thick phase retardation plate and polarisation of output pulses remains linear only in the case when the phase difference for the orthogonally polarised components along the beam path in the crystal is a multiple of 2π. In the experiments it was achieved by careful crystal alignment in the plane orthogonal to the phase-matching plane, which allowed changing the optical path lengths for the o- and e-beams.

Unavoidable losses in the nonlinear filter are easily compensated for in RA2. Pulses from RA1 after passing the PC were injected into RA2 and successively amplified up to level of ~100 μJ. A drop in the RA2 seed energy is compensated for by setting an additional roundtrip through the RA2 cavity. Thereby, the insertion of the PC had a minor influence on the RA2 output pulse energy, but improved markedly the amplified pulse contrast with respect to ASE. The high dynamic range cross correlation of pulses at the RA2 output is presented in Fig. 12. Without the PC the ASE intensity was at the level of 3×10^{-6} with respect to the main pulse intensity. Employments of a nonlinear filter lowered the ASE level by more than two orders (down to 10^{-8}) (Fig. 12a). Assuming that the ASE intensity distribution in the RA cavity is flat and the roundtrip time is 12 ns, we estimated the energy of the nanosecond background to be 1.2×10^{-4}% of the total output energy. Approximately the same contrast enhancement ratio was obtained also in the case when the RA1 seed pulse energy was lowered down to 0.12 pJ (Fig. 12b).

It is important to mention that the effect of polarisation rotation is different across the beam cross section. The presented experimental data on pulse contrast enhancement are integral parameters and indicate 'averaged across the beam' pulse quality improvement. Also we should note that a similar effect takes place in the temporal scale due to nonuniform degree of polarisation rotation along the pulse envelope. As a result, we have observed the decrease in the pulse duration by ~20% after the pulse cleaner. A more detailed investigation of the PC is given elsewhere [19]. Further pulse amplification in linear amplifiers leads to a slight drop in the main pulse/ASE contrast ratio because of gain saturation and spontaneous emission in active elements of the power amplifiers. At a maximum output energy of 600 mJ the ASE/pulse intensity ratio is $\sim 4 \times 10^{-8}$ (Fig. 12c).

5. Conclusions

We demonstrated a scheme of a direct Nd : YAG-amplification system seeded with femtosecond Yb : KGW pulses, realising all-optical synchronisation between picosecond pump and broadband OPCPA signals. The measured amplified picosecond pulse contrast value was 3×10^{-6}. By using multiple Fabry–Perot IEs, the femtosecond pulses from the Yb : KGW oscillator were stretched in time up to 100 ps without noticeable pulse envelope modulation. We showed by computer simulation and experiment that pulse envelope modulation could be severely reduced by inserting a second IE with the optimal base which is equal to half the thickness of the first one. We also demonstrated that pulse envelope modulation decreases with increasing second IE reflectivity. We presented a simple and reliable intensity dependent filter for contrast enhancement in the Nd : YAG amplification system. Picosecond pulse contrast enhancement by more than two orders and filter transmission up to 24% using the type-II KTP SHG crystal at incident pulse intensities of less than 1 GW cm^{-2} were demonstrated. As a result, we amplified 100-ps pulse up to energy of 600 mJ with a $\sim 4 \times 10^{-8}$ contrast value.

Acknowledgements. This work was financially supported by the Lithuanian State Science and Studies Foundation (Grant No. B-06/2009) and EC's Seventh Framework Programme (LASERLAB-EUROPE, Grant Agreement No. 228334). This work is also a part of national ELI-oriented activities.

References

1. Mourou G., Tajima T., Bulanov S.V. *Rev. Mod. Phys*., **78** (2), 309 (2006).
2. Herrmann D., Veisz L., Tautz R., Tavella F., Schmid K., Pervak V., Krausz F. *Opt. Lett*., **34** (16), 2459 (2009).
3. Adachi S., Ishii N., Kanai T., Kosuge A., Itatani J., Kobayashi Y., Yoshitomi D., et al. *Opt. Express,* **16** (19), 14341 (2008).

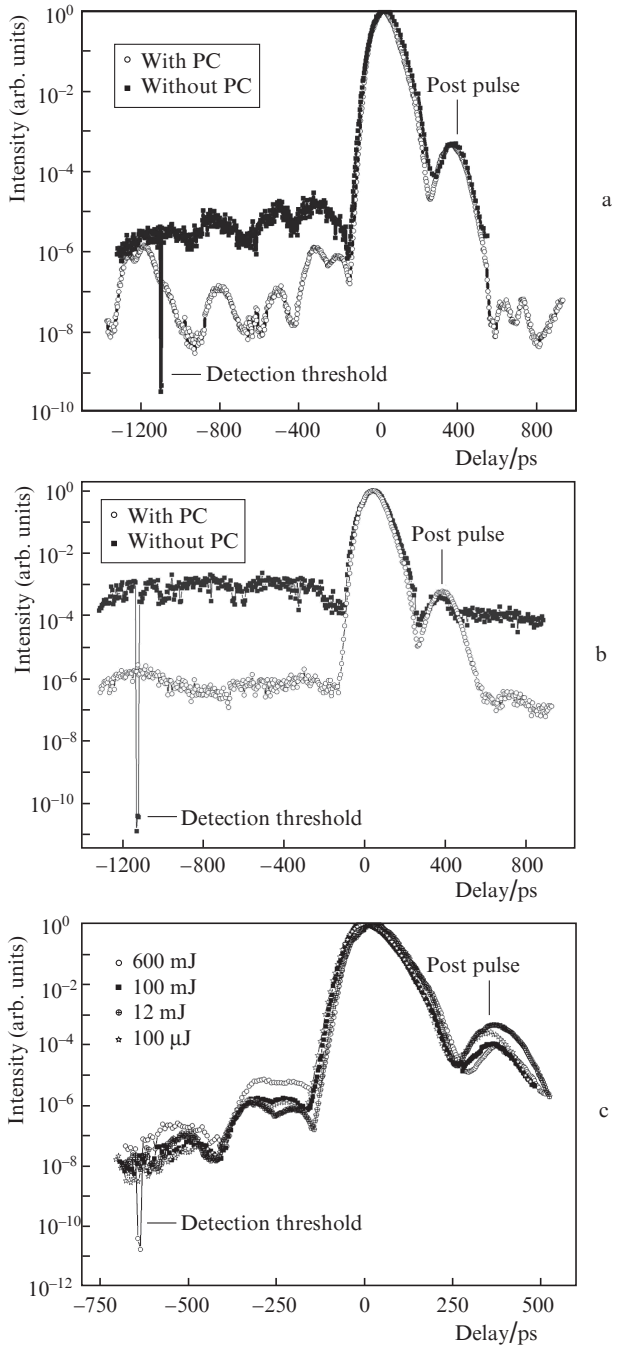

Figure 12. Third-order cross-correlation traces of amplified pulses: after RA2 at seed energy E_s = 12 pJ (a), after RA2 at seed energy E_s = 0.12 pJ (b), at the output of the entire system at E_s = 12 pJ and for different output pulse energies (c).

4. Ishii N., Teisset C.Y., Fuji T, Baltuska A., Krausz F. *Sel. Top. Quantum Electron*., **12** (2), 173 (2006).
5. Jovanovic I., Comaskey B. J., Ebbers C.A., Bonner R.A., Pennington D.M., Morse E.C. *Appl. Opt*., **41** (15), 2923 (2002).
6. Zeng H., Wu J., Xu H., Wu K., Wu E. *Appl. Phys. B*, **41** (7), 837 (2004).
7. Teisset C.Y., Ishii N., Fuji T., Metzger T., Köhler S., Holzwarth R., Baltuška A., Zheltikov A.M., Krausz F. *Opt. Express*, **13** (17), 6550 (2005).
8. Ross I.N., New G.H.C., Bates P.K. *Opt. Commun*., **273** (2), 510 (2007).
9. Mücke O.D., Sidorov D., Dombi P., Pugžlys A., Baltuška A., Ališauskas S., Smilgevičius V., et al. *Opt. Lett*., **34** (2), 118 (2009).
10. Lefort L., Barthelemy A. *Opt. Lett*., **20** (17), 1749(1995).
11. Leford L., Barthelemy A. *Electron. Lett*., **31** (11), 910 (1995).
12. Louis S., Couderc V., Louradour F., Faugeras P., Barthelemy A. *J. Opt. A: Pure Appl*., **3** (2), 139 (2001).
13. Louradour F., Mugnier A., Albert A., Couderc V., Barthelemy A. *Opt. Commun*., **188** (5-6), 333 (2001).
14. Yu Jin. *Appl. Phys. Lett*., **89** (18), 181107 (2006).
15. Bagnoud V., Begishev I.A., et al. *Opt. Lett*., **30** (14), 1843 (2005).
16. Auerbach J.M., Karpenko V.P. *Appl. Opt*., **33** (15), 3179 (1994).
17. Skeldon M.D., Bui S.T. *J. Opt. Soc. Am. B*, **10** (4), 677 (1993).
18. Martin W.E., Milam D. *Appl. Opt*., **15** (12), 3054 (1976).
19. Adamonis J., Antipenkov R., Kolenda J., Michailovas A., Piskarskas A., Varanavicius A. *Appl. Phys. B*, 106 (2), 321 (2012).